

A CAUTIONARY TALE: MARVELS BROWN DWARF CANDIDATE REVEALS ITSELF TO BE A VERY LONG PERIOD, HIGHLY ECCENTRIC SPECTROSCOPIC STELLAR BINARY

CLAUDE E. MACK III¹, JIAN GE², ROHIT DESHPANDE^{3,4}, JOHN P. WISNIEWSKI⁵, KEIVAN G. STASSUN^{1,6}, B. SCOTT GAUDI⁷, SCOTT W. FLEMING^{2,3,4}, SUVRATH MAHADEVAN^{3,4}, NATHAN DE LEE^{2,1}, JASON EASTMAN⁷, LUAN GHEZZI^{8,9}, JONAY I. GONZÁLEZ HERNÁNDEZ^{10,11}, BRUNO FEMENÍA^{10,11}, LETÍCIA FERREIRA^{12,9}, GUSTAVO PORTO DE MELLO^{12,9}, JUSTIN R. CREPP¹³, DANIEL MATA SÁNCHEZ^{10,11}, ERIC AGOL¹⁴, THOMAS G. BEATTY⁷, DMITRY BIZYAEV¹⁵, HOWARD BREWINGTON¹⁵, PHILLIP A. CARGILE¹, LUIZ N. DA COSTA^{8,9}, MASSIMILIANO ESPOSITO^{10,11}, GARRET EBELKE¹⁵, LESLIE HEBB^{1,14}, PENG JIANG², STEPHEN R. KANE¹⁶, BRIAN LEE², MARCIO A. G. MAIA^{8,9}, ELENA MALANUSHENKO¹⁵, VICTOR MALANUSHENKO¹⁵, DANIEL ORAVETZ¹⁵, MARTIN PAEGERT¹, KAIKE PAN¹⁵, CARLOS ALLENDE PRIETO^{10,11}, JOSHUA PEPPER¹, RAFAEL REBOLO^{10,11}, ARPITA ROY³, BASÍLIO X. SANTIAGO^{17,9}, DONALD P. SCHNEIDER^{3,4}, AUDREY SIMMONS¹⁵, ROBERT J. SIVERD¹, STEPHANIE SNEDDEN¹⁵, AND BENJAMIN M. TOFFLEMIRE¹⁸

¹ Department of Physics and Astronomy, Vanderbilt University, Nashville, TN 37235, USA; claud.e.mack@vanderbilt.edu

² Department of Astronomy, University of Florida, 211 Bryant Space Science Center, Gainesville, FL, 32611-2055, USA

³ Department of Astronomy and Astrophysics, The Pennsylvania State University, University Park, PA 16802, USA

⁴ Center for Exoplanets and Habitable Worlds, Pennsylvania State University, University Park, PA 16802, USA

⁵ Homer L Dodge Department of Physics & Astronomy, University of Oklahoma, 440 W Brooks St, Norman, OK 73019, USA

⁶ Department of Physics, Fisk University, Nashville, TN, USA

⁷ Department of Astronomy, The Ohio State University, 140 West 18th Avenue, Columbus, OH 43210, USA

⁸ Observatório Nacional, Rua Gal. José Cristino 77, Rio de Janeiro, RJ 20921-400, Brazil

⁹ Laboratório Interinstitucional de e-Astronomia—LineA, Rio de Janeiro, RJ 20921-400, Brazil

¹⁰ Instituto de Astrofísica de Canarias (IAC), E-38205 La Laguna, Tenerife, Spain

¹¹ Departamento de Astrofísica, Universidad de La Laguna, E-38206 La Laguna, Tenerife, Spain

¹² Observatório do Valongo, Universidade Federal do Rio de Janeiro, Rio de Janeiro, RJ 20080-090, Brazil

¹³ Department of Physics, University of Notre Dame, 225 Nieuwland Science Hall, Notre Dame, IN 46556, USA

¹⁴ Astronomy Department, University of Washington, Box 351580, Seattle, WA 98195, USA

¹⁵ Apache Point Observatory, P. O. Box 59, Sunspot, NM 88349-0059, USA

¹⁶ NASA Exoplanet Science Institute, Caltech, MS 100-22, 770 South Wilson Avenue, Pasadena, CA 91125, USA

¹⁷ Instituto de Física, UFRGS, Caixa Postal 15051, Porto Alegre, RS 91501-970, Brazil

¹⁸ Astronomy Department, University of Wisconsin-Madison, 475 N Charter St, Madison, WI 53706, USA

Published in *The Astronomical Journal*, 145:139, 2013 May

ABSTRACT

We report the discovery of a highly eccentric, double-lined spectroscopic binary star system (TYC 3010-1494-1), comprising two solar-type stars that we had initially identified as a single star with a brown dwarf companion. At the moderate resolving power of the MARVELS spectrograph and the spectrographs used for subsequent radial-velocity (RV) measurements ($R \lesssim 30,000$), this particular stellar binary mimics a single-lined binary with an RV signal that would be induced by a brown dwarf companion ($M \sin i \sim 50 M_{\text{Jup}}$) to a solar-type primary. At least three properties of this system allow it to masquerade as a single star with a very low-mass companion: its large eccentricity ($e \sim 0.8$), its relatively long period ($P \sim 238$ days), and the approximately perpendicular orientation of the semi-major axis with respect to the line of sight ($\omega \sim 189^\circ$). As a result of these properties, for $\sim 95\%$ of the orbit the two sets of stellar spectral lines are completely blended, and the RV measurements based on centroiding on the apparently single-lined spectrum is very well fit by an orbit solution indicative of a brown dwarf companion on a more circular orbit ($e \sim 0.3$). Only during the $\sim 5\%$ of the orbit near periastron passage does the true, double-lined nature and large RV amplitude of $\sim 15 \text{ km s}^{-1}$ reveal itself. The discovery of this binary system is an important lesson for RV surveys searching for substellar companions; at a given resolution and observing cadence, a survey will be susceptible to these kinds of astrophysical false positives for a range of orbital parameters. Finally, for surveys like MARVELS that lack the resolution for a useful line bisector analysis, it is imperative to monitor the peak of the cross-correlation function for suspicious changes in width or shape, so that such false positives can be flagged during the candidate vetting process.

Subject headings: binaries: spectroscopic – brown dwarfs – stars: individual (TYC 3010-1494-1)

1. INTRODUCTION

As a part of the third phase of the Sloan Digital Sky Survey (SDSS-III; Eisenstein et al. 2011), the MARVELS (Multi-object APO Radial Velocity Exoplanet Large-area Survey) project is searching for substellar companions by monitoring the radial velocities (RVs) of 3330 FGK stars (Ge et al. 2008, 2009; Ge & Eisenstein 2009). This sample size is large enough for the project to find relatively rare objects, such as brown dwarf

(BD) companions to solar-type stars. The paucity of observed BD companions to solar-type stars with separations of $\lesssim 5$ AU is typically referred to as the BD desert (Marcy & Butler 2000). Since the size of the MARVELS sample allows us to begin to quantify how arid the BD desert may be, any MARVELS discovery of a BD in the desert (or lack thereof) is a step toward increasing our understanding of BD formation.

In addition to its large homogeneous target sam-

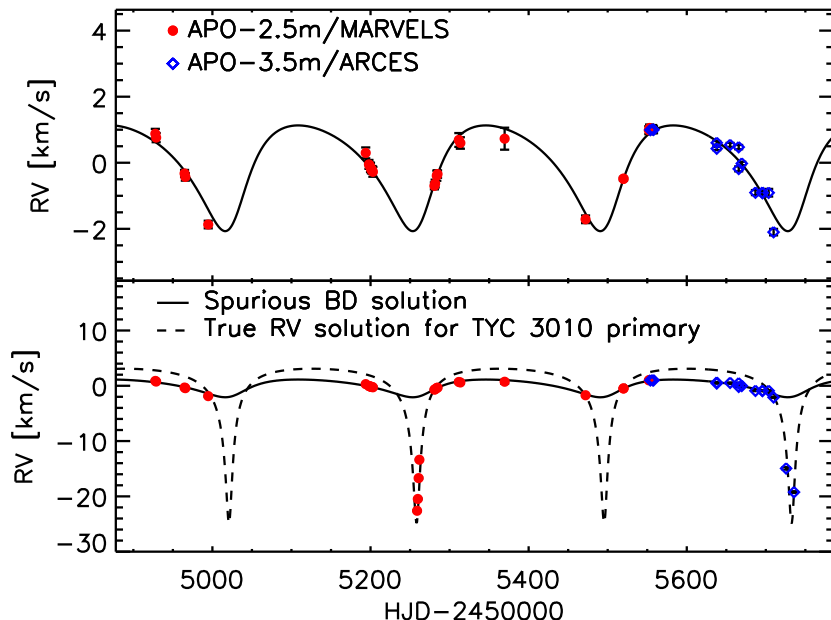


FIG. 1.— The radial velocity data obtained with the MARVELS (red) and ARCES (blue) spectrographs at the time that we began to suspect that TYC 3010 was a double-lined spectroscopic binary (SB2) instead of a brown dwarf (BD) companion to a solar-type star. In the top panel, we show the EXOFAST fit (solid line; Eastman et al. 2013) to the low-amplitude RV variations that are observed when the binary is away from periastron. This solution corresponds to a substellar companion in the BD regime ($M \sin i \sim 50 M_{\text{Jup}}$) orbiting a solar-type primary with a period of ~ 238 days. In the bottom panel, we include the high-amplitude MARVELS (red points near HJD 2455250) and ARCES (blue points near HJD 2455730) outliers that were initially thought to be spurious, as well as the final, true RV curve (dashed line) for the primary component of the SB2. For both spectrographs, the majority of the data agrees well with the BD solution, and it is tempting to suspect the outliers as spurious. However, upon investigating the cross-correlation function (CCF) for these outliers, the CCFs show strong evidence for a secondary stellar component (see Figure 3). With the HET/HRS spectrograph we were able to completely cover periastron and confirm that the system is indeed a double-lined spectroscopic binary because these points actually correspond to the flux-weighted average of the true primary and secondary RVs. To perform the double-lined fit for these (apparently) single-lined epochs, we first disentangled the primary and secondary components as described in Section 3.2.1.

ple, MARVELS differs from other surveys for substellar companions in two key ways. First, the project employs a dispersed fixed-delay interferometer (DFDI; Ge 2002; Ge et al. 2002; Erskine 2003; Ge et al. 2006; van Eyken et al. 2010; Wang et al. 2011). Second, it uses a multi-object spectrograph to observe 60 stars simultaneously (Ge et al. 2009). The DFDI prototype instrument was used to discover the first extrasolar planet around HD 102195 in 2006 with this new RV method (Ge et al. 2006). The MARVELS DFDI technique combines an interferometer with a medium resolution spectrograph ($R \sim 12,000$) in order to obtain a precision of $\sim 100 \text{ m s}^{-1}$. Given its RV precision and survey design to monitor each target with at least 24 RV measurements over at least 1 yr, MARVELS is sensitive to BD and low-mass stellar companions with periods ranging from a few days to hundreds of days. Nonetheless, certain specific types of astrophysical false positives can mimic substellar companions unless additional vetting is performed. This paper describes just such a case, TYC-3010-1494-1 (hereafter TYC 3010), a stellar binary that initially appeared as a single star with a substellar companion and that, through a confluence of orbital parameters, continued to masquerade as such despite a disconcertingly extensive amount of observation and analysis.

When we began analysis of TYC 3010, MARVELS and its pilot project had already detected two BD candidates orbiting late F stars in the BD desert (Fleming et al. 2010; Lee et al. 2011, at present, we have three more candidates in the desert: Ma et al. 2013; Jiang et al. 2013;

De Lee et al. 2013). The MARVELS discovery data indicated that TYC 3010 possessed a substellar companion with a minimum mass of $\sim 50 M_{\text{Jup}}$ and that it was on a ~ 238 -day moderately eccentric orbit with an RV amplitude of $\sim 1.5 \text{ km s}^{-1}$ (see the top panel of Figure 1). However, given the cadence of MARVELS and the period of the orbit, there were significant gaps in the phase coverage and additional observations with a different spectrograph were required to constrain the RV solution. Initially, the follow-up data remained fully consistent with the BD companion scenario. However, during the course of the program, we found two RV points that were shifted by $\sim 20 \text{ km s}^{-1}$ with respect to most of our data; while investigating the source of these anomalous points, we realized that a few similar points had been rejected from our MARVELS discovery data by the team’s outlier rejection procedures (see bottom panel of Figure 1). Examining the cross-correlation function (CCF) of the anomalous RV points (in both the discovery and subsequent data) revealed evidence that there were two components in the CCF, which suggested that the companion to the primary was most likely a stellar-mass secondary. Finally, including the initially flagged outlier measurements and disentangling the RV measurements of the two components, the system was found to be a nearly equal-mass stellar binary ($q \sim 0.88$) on a highly eccentric orbit ($e \sim 0.8$). Evidently, for a system like TYC 3010, it is possible to clip just a few measurements and obtain an apparently reasonable solution that is convincing but completely incorrect.

As large scale RV and transit surveys for exoplanets become more common, it is increasingly inevitable that any and all forms of astrophysical false positives, despite their rarity, will be found. Indeed, the first BD candidate discovered by the MARVELS project, MARVELS-1 (Lee et al. 2011), appeared to exhibit evidence for an additional planet-mass companion, but turned out instead to likely be a quadruple system, comprising four stars with no detected BD or planetary-mass companion (Wright et al. 2013). Akin to TYC 3010, MARVELS-1 is a double-lined spectroscopic binary; the stars have relative RVs which are sufficiently low that they are always blended, even at the resolution of the Hobby-Eberly Telescope (HET; $R \sim 60,000$ mode). Thus, with both MARVELS-1 and TYC 3010, we actually measure a flux-weighted mean of two sets of stellar spectral lines. This flux-weighted mean exhibits a suppressed velocity shift that mimics a single-lined binary with a BD secondary. Both systems possess geometries that allow them to masquerade as less massive systems: MARVELS-1 is nearly face-on, which leads to low projected velocities, while TYC 3010 is on a highly elliptical orbit with a semi-major axis oriented nearly perpendicular to our line of sight.

Similarly, Mandushev et al. (2005) describe what at first appeared to be a transiting BD companion to an F star from the TRES transit survey, but turned out instead to be an F star blended with a G+M stellar eclipsing binary. The system that we describe here follows these unfortunate examples, and is similarly pernicious.

In the following sections, we present our analysis as a kind of cautionary tale for other RV surveys to avoid similar false positives. In Section 2, we describe the spectroscopic and photometric data obtained for TYC 3010. In Section 3, we discuss in detail the nature of the evidence that led us to conclude that TYC 3010 was an eccentric stellar binary instead of a BD companion to a solar-type star. We also present the properties we derived for both components of the spectroscopic binary. In Section 4, we discuss the circumstances that allowed this false positive to masquerade for so long and through several vetting steps as a compelling detection of a substellar companion, and we describe methods that the MARVELS team and other RV surveys can use to recognize this kind of astrophysical false positive in the future. Finally, in Section 5, we conclude with a summary of the main results.

2. OBSERVATIONS AND DATA PROCESSING

We obtained a total of 65 RV measurements from the Sloan 2.5m, the APO 3.5m, and the HET 9.2m telescopes. We will briefly summarize the characteristics of the data from all three telescopes. For more details of the analysis, please see Fleming et al. (2010), Lee et al. (2011), and Wisniewski et al. (2012).

2.1. SDSS-III MARVELS Discovery RV Data

A total of 28 spectra (see Table 1) of TYC 3010 were obtained with the Sloan 2.5m telescope (Gunn et al. 2006) at Apache Point Observatory (APO). The multi-fiber MARVELS spectrograph (Ge et al. 2009) can simultaneously measure the RVs of 60 stars during each telescope pointing. Both beams of the interferometer are imaged onto the detector, so each 50-minute observation results in two fringed spectra in the wavelength range

TABLE 1
OBSERVED HELIOCENTRIC SINGLE-LINED
RADIAL VELOCITIES FOR TYC 3010

HJD	Instrument ^a	RV (km s ⁻¹)	σ_{RV} (km s ⁻¹)
2454927.82470	M	62.681	0.148
2454928.85061	M	62.564	0.139
2454964.76792	M	61.479	0.108
2454965.77714	M	61.374	0.113
2454994.69536	M	59.933	0.115
2455193.91250	M	62.102	0.165
2455197.96727	M	61.753	0.134
2455198.94828	M	61.714	0.095
2455199.96552	M	61.664	0.139
2455200.98947	M	61.585	0.097
2455201.97760	M	61.587	0.116
2455202.99063	M	61.528	0.149
2455258.88272	M	39.192	0.091
2455259.83118	M	41.327	0.092
2455260.82412	M	45.097	0.145
2455261.82050	M	48.416	0.096
2455280.77587	M	61.103	0.105
2455280.76844	M	61.174	0.117
2455283.81484	M	61.411	0.154
2455284.75054	M	61.461	0.112
2455311.68421	M	62.493	0.209
2455313.62591	M	62.402	0.174
2455369.64423	M	62.531	0.333
2455551.99403	M	62.788	0.120
2455552.98222	M	62.856	0.104
2455553.98561	M	62.795	0.121
2455556.97163	M	62.821	0.123
2455557.97465	M	62.801	0.104
2455471.98302	A	60.138	0.116
2455519.95995	A	61.359	0.052
2455519.98157	A	61.371	0.051
2455637.88366	A	62.452	0.055
2455637.92209	A	62.278	0.048
2455654.83350	A	62.390	0.059
2455665.65219	A	62.323	0.065
2455665.69165	A	61.664	0.075
2455669.60113	A	61.827	0.052
2455686.82409	A	60.946	0.076
2455695.66512	A	60.949	0.039
2455695.70529	A	60.931	0.053
2455703.61994	A	60.942	0.116
2455709.77767	A	59.749	0.098
2455903.90846	H	62.448	0.051
2455917.87269	H	62.237	0.060
2455928.84083	H	61.759	0.046
2455940.80855	H	61.122	0.058
2455946.80490	H	60.285	0.055
2455950.80134	H	59.539	0.045
2455953.82447	A	58.385	0.049
2455954.00566	H	58.467	0.050

NOTE. — The ARCES and HRS RV values were measured as absolute heliocentric RVs, while the MARVELS discovery data were measured on a relative instrumental scale; the MARVELS RVs have been offset to the same (heliocentric) scale as the ARCES and HRS measurements.

^a Instruments: MARVELS (M), ARCES (A), and HRS (H) spectrographs.

of ~ 500 – 570 nm with a resolving power of $R \sim 12,000$. The MARVELS interferometer delay calibrations are described in Wang et al. (2012a,b). For more details on how the data were reduced and analyzed to yield RVs, see Lee et al. (2011).

As described below, it proved essential to examine the CCFs of the individual spectra. However, performing a cross-correlation on a DFDI spectrum requires a few steps beyond what one performs for a typical slit or cross-dispersed echelle spectrograph. In both cases the images are reduced using standard techniques (bias subtraction,

TABLE 2
OBSERVED HELIOCENTRIC DOUBLE-LINED RADIAL VELOCITIES FOR TYC 3010

HJD	Instrument ^a	RV _{primary} (km s ⁻¹)	σ _{RV,primary} (km s ⁻¹)	RV _{secondary} (km s ⁻¹)	σ _{RV,secondary} (km s ⁻¹)
2455725.68377	A	46.012	0.167	75.222	0.257
2455735.62781	A	43.197	0.251	81.056	0.175
2455956.76037	H	53.788	0.030	69.104	0.063
2455959.78075	H	51.409	0.025	71.807	0.055
2455964.75592	H	44.163	0.026	80.066	0.055
2455964.83117	A	44.884	0.071	79.700	0.372
2455967.75334	H	36.755	0.030	88.389	0.062
2455967.82824	A	37.684	0.076	88.651	0.471
2455968.74640	H	34.456	0.025	90.966	0.054
2455971.73989	H	36.359	0.029	88.685	0.060
2455972.97350	H	40.368	0.025	84.354	0.054
2455976.73787	H	50.072	0.024	73.253	0.051
2455977.71541	H	51.788	0.028	71.580	0.058
2455978.71767	H	52.990	0.026	69.840	0.056
2455979.71599	H	54.160	0.029	68.450	0.062

^a Instruments: ARCES (A) and HRS (H) spectrographs.

trace correction, flat fielding etc.) Once a fully processed two-dimensional spectrum has been extracted, there is a divergence in the techniques. In the case of a normal spectrum, one merely sums the flux in the slit (channel) direction to produce a one-dimensional spectrum. This approach is not possible in the DFDI technique because the fringing pattern will introduce false fluctuations in total flux if one just sums in the slit direction. These fluctuations will be a function of the phase of the fringe pattern in each pixel channel. To correct for this effect, a sinusoidal function of the form $A \sin(wx + b) + c$ is fit to each pixel column. For the purposes of cross-correlation the only term of interest is c , or the mean flux in each channel. A one dimensional spectrum is then constructed using the c term in each channel. From this point forward the CCF is determined using standard techniques.

2.2. APO-3.5m/ARCES RV Data

A total of 19 RV observations were taken with the APO 3.5m telescope using the ARC Echelle Spectrograph (ARCES; Wang et al. 2003). This spectrograph operates in the optical regime from $\sim 3,600$ – $10,000 \text{ \AA}$ with a resolving power of $R \sim 31,500$. The first set of observations were taken from 2010 October to 2011 June. The second set of observations, which were undertaken with the goal of increasing phase coverage of periastron, were obtained during 2012 January–February. As shown in Tables 1 and 2, there were 15 ARCES points observed outside of periastron, and 4 points during periastron (The first two of these periastron points are where we initially resolved both the primary and secondary spectral lines—see bottom panel of Figures 1, 2, and 3—and began to suspect that the system might be a double-lined spectroscopic binary).

To achieve high-accuracy RV measurements with the echelle spectrograph, we obtained a Thorium-Argon (ThAr) exposure after every science exposure. In order to place TYC 3010 on an absolute RV scale, we also frequently bracketed our observations of TYC 3010 with observations of the RV standard HD 102158, which has an absolute RV of 28.122 km s^{-1} (Crifo et al. 2010; Nidever et al. 2002). From the standard deviation of the 13 RV measurements we obtained for HD 102158 (see Table 3), we were able to determine that the ARCES

spectrograph possesses an RV stability of $\sim 0.5 \text{ km s}^{-1}$.

Two of the ARCES spectra were taken with longer exposure times in order to achieve a high signal-to-noise ratio (S/N) for deriving the fundamental stellar parameters (see Section 3.2.2). These two spectra were taken with an exposure time of 200 s and with the default slit setting described in Wisniewski et al. (2012). The data were reduced with IRAF, and after barycentric corrections and continuum normalization, the two spectra were combined to produce a final spectrum with an S/N of ~ 170 per resolution element at $\sim 6500 \text{ \AA}$. However, once we realized that TYC 3010 was a double-lined spectroscopic binary, we re-derived the spectroscopic parameters with a double-lined spectrum obtained near periastron, as described in Section 3.2.2.

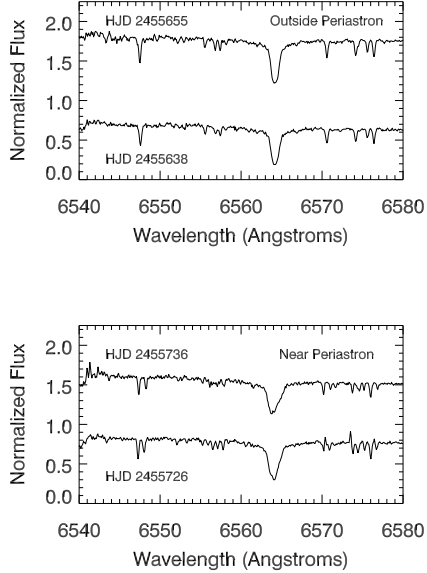


FIG. 2.— (Top) Outside periastron the combined spectrum appears convincingly single-lined. (Bottom) Near periastron the spectrum is resolved into its double-lined components (with the ARCES and HRS spectrographs, but not MARVELS). We used the double-lined spectrum with highest S/N when we were deriving the properties of the two stars via spectral characterization.

2.3. HET/HRS RV Data

Upon realizing the eccentric binary-star nature of the object from the APO 3.5m data, observations were initiated with the 9.2m HET (Ramsey et al. 1998) and the Higharcsec Resolution Spectrograph (HRS; Tull 1998) at a resolving power of $R \sim 30,000$ using a 2 arcsec optical fiber. A total of 18 observations were obtained to completely cover periastron, and thereby fully constrain the orbit. The queue-scheduled observing mode of the HET (Shetrone et al. 2007) is extremely well suited for investigating objects that require monitoring over a long timespan, as well as targeted observations near periastron passage. For wavelength calibration, ThAr images were obtained immediately before and after the science exposure to aid in calibrating any possible instrument drift. The data were reduced and wavelength calibrated using custom optimal extraction scripts written in IDL. RVs were measured using two different techniques, which we describe below. The HET observations clearly resolve the orbit for TYC 3010, and constrain the eccentricity to a value of $e \sim 0.8$ (see Section 3.2).

2.3.1. CCF Mask

RVs were measured using a cross-correlation mask derived from National Solar Observatory Fourier transform spectroscopic solar data (Lytle 1993), and a technique similar to that described by Baranne et al. (1996). The resultant CCF encodes information from the $\sim 400\text{--}600$ nm region, and we elected not to use redder wavelengths due to issues with telluric contamination. Figure 3 shows the resulting CCF for an epoch during periastron and one outside of periastron; as is the case for the ARCES data,

TABLE 3
OBSERVED HELIOCENTRIC RADIAL VELOCITIES FOR
THE RV STANDARD HD102158

HJD	RV (km s ⁻¹)	σ_{RV} (km s ⁻¹)
2455654.81577	28.734	0.052
2455665.67180	28.050	0.034
2455665.71479	28.169	0.043
2455669.58461	27.736	0.045
2455686.80825	27.470	0.054
2455695.68591	28.030	0.038
2455695.72570	28.090	0.034
2455703.60341	28.244	0.039
2455709.76151	27.476	0.030
2455725.66705	26.692	0.123
2455735.61237	28.126	0.109
2455964.81467	28.093	0.058
2455967.81369	27.728	0.050

during periastron the primary and secondary peaks are clearly visible in the HET CCFs, but outside of periastron only a single peak is resolved. The centroid of the CCF peak is determined by fitting a Gaussian.

This technique has been used successfully for isolated stars to derive precise RVs by the teams using fiber-fed high resolution spectrographs (e.g., HARPS, SOPHIE, ELODIE, CORALIE; Pepe et al. 2000; Bouchy 2006; Baranne et al. 1996; Queloz et al. 2000), since PSF stability is an important component of deriving precise RVs with this technique. Any mismatch between the CCF and the simple Gaussian model is absorbed as a zero-point offset in the derived RVs as long as the PSF is stable (resulting in a stable CCF shape). The HET/HRS spectrograph is also fiber-fed, enabling this technique to also be applied to binary stars. This method is computationally efficient, and also does not require that the spectra be normalized, resulting in a quick turn around in determining RVs once the data are in hand. The RVs derived enabled us to plan and obtain observations as soon as the peaks began to separate on the approach to peri-passage. Table 1 shows the HET RVs obtained with this technique for those epochs where the CCF appears as a single peak.

2.3.2. TODCOR

While the CCF Mask technique described above works quite well, it does not yield the best RVs possible for spectra with two CCF peaks since only one mask (G2 spectral type) was used in determining peak positions. Once all the data were in hand, we were able to apply the two-dimensional cross-correlation algorithm, TODCOR (Zucker & Mazeh 1994). TODCOR can simultaneously cross-correlate two stellar templates against a blended target stellar spectrum to disentangle the stellar RVs of the components as well as derive a flux ratio. We used TODCOR along with HRS observations of HD161237 (G5V) and HD 198596 (K0V) as templates to measure the RVs of TYC 3010. The HRS spectrum was divided into different bandpasses, and each bandpass was solved independently following Zucker (2003) and the resulting cross-correlation surface combined with a maximum likelihood analysis. Further details on our implementation of the TODCOR algorithm, as well as details of our custom HRS spectral extraction pipeline, can be found in Bender et al. (2012).

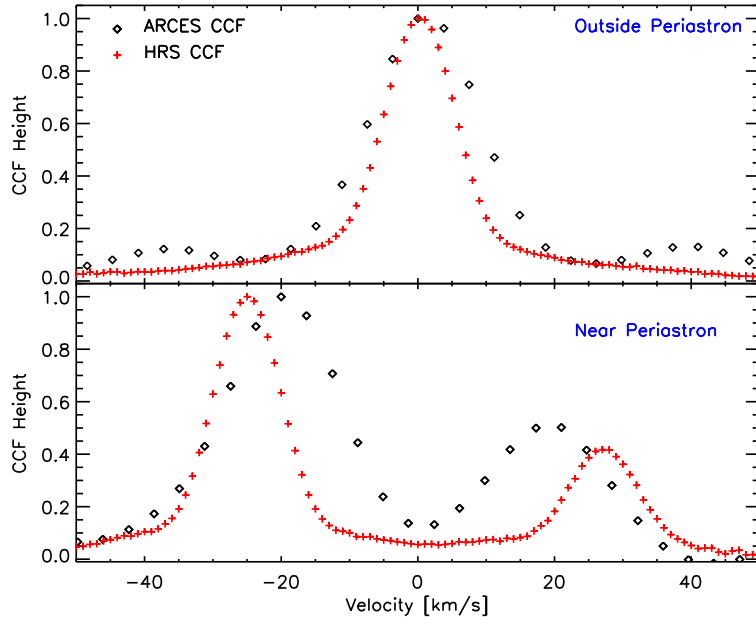


FIG. 3.— Example CCFs obtained with the ARCES and HRS spectrographs from similar (but different) phases outside of periastron (*top panel*) and during periastron (*bottom panel*). Since most of the data were obtained outside of periastron, most of the RV points correspond to single-peak CCFs. However, for data from near periastron, the ARCES and HRS spectrographs are able to resolve two peaks. The secondary peak is comparable in height to the primary peak, which led us to suspect that TYC 3010 is an eccentric spectroscopic binary with the semi-major axis aligned perpendicular to the line of sight (see Figure 8). With this configuration, we would only resolve two peaks in the CCF if we happen to catch the pair of stars as they briefly pass through periastron. To confirm this interpretation, we fully observed periastron with HET/HRS, which allowed us to completely constrain the orbit (see Figure 7).

Table 2 shows the RVs of the primary and secondary determined using this algorithm at those epochs where the CCF is double peaked. We add 0.05 km s^{-1} in quadrature to the TODCOR formal errors to account for additional noise effects like wavelength calibration, small tracking induced PSF changes, etc. While the HET observed the target on 18 epochs, the secondary RVs are only reliably measured for 11 epochs. These are the epochs where the primary and secondary peaks are sufficiently separated to determine an independent RV for each. While RVs can be determined for the other 7 epochs, they are RVs of blended spectra, and the associated systematic error is not only larger, but also more difficult to quantify.

Since both peaks are unambiguously detected in TODCOR at these epochs, we are also able to measure the secondary to primary flux ratio, α , which we determine to be $\alpha = 0.335 \pm 0.035$ by averaging the flux ratio of the templates (G5V and K0V) over four bandpasses spanning 4663–5863 Å. Finally, the mass ratio derived from these 11 epochs is $q \sim 0.88$.

2.4. FastCam Lucky Imaging

The MARVELS team obtained lucky imaging for TYC 3010 in order to detect any spatially resolvable companions. In 2011 April, using the FastCam (Oscz et al. 2008) instrument on the 1.5m TCS telescope at Observatorio del Teide in Spain, we obtained 47,000 frames in the *I*-band with a 70 ms exposure time for each frame. Data processing was accomplished with a custom-made IDL pipeline.

As described in Fleming et al. (2012), the best frames

are selected via the brightest pixel (BP) method. The frames with the brightest $X\%$ of BPs are combined to generate a final image, where $X = \{1, 5, 15, 30, 50, 80\}$ for TYC 3010. Figure 4 shows the resulting final images for each particular percentage of the best frames.

No companions are detected, but we can place constraints on the upper limit of the masses of resolvable companions. Using the spectroscopic T_{eff} for TYC 3010 (see Section 3.2.2), and the relations from Mamajek et al. (2011), we determine the bolometric magnitude. Combining the bolometric magnitude with mass–luminosity relations (Henry et al. 1999; Henry 2004; Delfosse et al. 2000; Xia et al. 2008; Xia & Fu 2010), we convert the detection limit for the *I*-band magnitude into a lower limit for the masses of detectable companions at different separations. At the 5σ level, where σ is defined in Femenía et al. (2011) as the rms of the counts within concentric annuli centered on TYC 3010, and using 8 pixel boxes, we can rule out the presence of detectable companions above a mass of $\sim 0.35 M_{\odot}$ outside of 50 AU (see Figure 5).

2.5. Keck AO Imaging

In addition to the lucky imaging, we were also able to obtain adaptive optics (AO) images of TYC 3010 on 2012 October 21 UT using the NIRC2 imager at Keck (instrument PI: Keith Matthews; Matthews & Soifer 1994). Observations consist of a sequence of nine dithered frames in the *K'* filter (central $\lambda = 2.12 \mu\text{m}$) using the narrow camera (plate scale = 10 mas pix^{-1}) setting. Each frame consisted of 20 coadds with 0.1814 s of integration time per coadd, totaling 32.65 s of on-source exposure time. Images were processed using stan-

ard techniques to remove hot pixels, subtract the sky-background, and align and coadd the cleaned frames. No candidate companions were identified in either raw or processed images. Figure 5 shows our sensitivity to off-axis sources as a function of angular separation. Our diffraction-limited observations rule out the presence of companions 6.5 magnitudes fainter than the primary star for separations beyond $0.5''(5\sigma)$. Using theoretical isochrones from (Girardi et al. 2002), we convert this magnitude limit to a mass upper limit, as shown in Figure 5; we can exclude companions with a mass above $0.13 M_{\odot}$ outside of 100 AU.

3. RESULTS

In this section we present the orbit solution of the TYC 3010 system. First we show how the data initially suggested a spurious solution in which TYC 3010 is a single star with a BD companion. Next we present the correct solution, in which TYC 3010 is shown to be a double-lined spectroscopic stellar binary (SB2) with two solar-type stars, and we provide a full characterization of the system properties.

3.1. Initial spurious solution: a BD companion to a solar-type star

Of the 28 RV measurements collected with the MARVELS instrument, 24 passed the data quality checks and were therefore included in the automated orbit solution fitting procedures. For the ARCES data, the first 14 consecutive RV points obtained during the initial set of observations were fully consistent with our working solution, that TYC 3010 was a candidate BD (see Figure 1 and Table 4). These RV points are well fit by a solution consistent with a substellar object ($M \sin i \sim 50 M_{\text{Jup}}$) orbiting in the BD desert around a solar-type star. A robust fit to the low amplitude ($\sim 1\text{--}2 \text{ km s}^{-1}$) variations was found with the EXOFAST program (Eastman et al. 2013), which uses a set of Markov Chain Monte Carlo trials to find the best fit. This solution, shown in Figure 1 (top panel), is a very convincing fit to the 38 originally included MARVELS (red points) and APO (blue points) measurements. This fit yielded a χ^2 of 34.63 after scaling the error bars to force $\chi^2/\text{dof} \sim 1$. These scalings were not unreasonable compared to other MARVELS candidates.

As noted previously, four of the original MARVELS RV measurements were initially rejected as outliers. The outlier rejection procedure included a 40σ statistical clipping to avoid phase wrapping, and rejection of consecutive points deviating by a large systematic offset from the bulk of the measurements. The latter rejection step was specifically implemented in an attempt to account for cases of fiber mis-pluggings, which are known to happen on occasion, in which the wrong star is observed for a few observations in a row and those few measurements appear at a very different systemic velocity relative to the majority of the measurements. The four rejected MARVELS measurements are also shown in Figure 1 (bottom panel, red points) near HJD 2455250. The final (correct) orbit solution is also shown (see details below), but it must be noted that this final orbit solution is only a good fit after properly disentangling the RVs from epochs where just a single set of spectral lines is resolved; it is not a good fit to the *directly observed* single-lined RV

TABLE 4
TYC 3010 ORBITAL PARAMETERS: SPURIOUS
AND TRUE RV SOLUTIONS

	Spurious solution	True solution
T_P (BJD _{TDB} - 2450000)	$5496.8^{+1.8}_{-2.0}$	5970.04 ± 5.1
P (days)	$238.49^{+0.73}_{-0.70}$	237.96 ± 0.04
e	$0.384^{+0.067}_{-0.048}$	0.785 ± 0.003
ω (deg)	$200.88^{+2.35}_{-2.58}$	188.86 ± 0.67
K_1 (km s ⁻¹)	$1.970^{+0.240}_{-0.130}$	15.38 ± 0.25
K_2 (km s ⁻¹)	...	17.50 ± 0.16
γ (km s ⁻¹)	$61.759^{+0.077}_{-0.087}$	61.28 ± 0.09
$q = M_B/M_A$...	0.88 ± 0.02

NOTE. — The spurious solution consists of the EXOFAST (Eastman et al. 2013) fit to the MARVELS and ARCES RV data, excluding the points initially thought to be invalid outliers. The true solution was determined with the BINARY software (Gudehus 2001) and the MARVELS, ARCES, and HRS observations. For the true (SB2) solution, the single-lined RV measurements were disentangled into their primary and secondary components (see Section 3.2.1).

TABLE 5
CATALOG PROPERTIES OF TYC 3010-1494-1

Parameter	Value	Uncertainty	Reference
α (2000)	11 00 11.45		(1)
δ (2000)	+39 43 24.74		(1)
pmRA [mas yr ⁻¹]	-43.4	1.7	(1)
pmDE [mas yr ⁻¹]	3.3	1.6	(1)
B_T	13.102	0.297	(1)
V_T	11.758	0.143	(1)
B	12.007	0.153	(2)
V	11.367	0.145	(2)
I_C	10.531	0.074	(2)
g	11.579	0.177	(2)
r	11.093	0.089	(2)
i	10.870	0.127	(2)
J	9.977	0.021	(3)
H	9.554	0.016	(3)
K_s	9.488	0.019	(3)
WISE1 (3.4 μm)	9.407	0.006	(4)
WISE2 (4.6 μm)	9.482	0.006	(4)
WISE3 (12 μm)	9.470	0.038	(4)

REFERENCES. — (1) Høg et al. (2000), (2) Henden et al. (2012), (3) Cutri et al. (2003), (4) Wright et al. (2010)

measurements, since these are in fact a flux-weighted average of the true primary and secondary RVs. The six “outlier” measurements from this first set of observations (four MARVELS points and two ARCES points) appear systematically displaced by $15\text{--}20 \text{ km s}^{-1}$ relative to the other 38 measurements, which are well fit by the spurious orbit (solid curve) but not by the correct orbit (dashed curve).

In addition, as we have done with all MARVELS candidates, we performed a fit to the spectral energy distribution (SED) of the system to verify that it is consistent with a single stellar source and to provide a consistency check on the spectroscopically determined stellar properties (see below). We constructed the SED using fluxes (see Table 5) from the Tycho catalogue (Høg et al. 2000), APASS (AAVSO Photometric All-Sky Survey; Data Release 6, see Henden et al. 2012), Two Micron All Sky Survey (Cutri et al. 2003), and WISE (Wright et al. 2010).

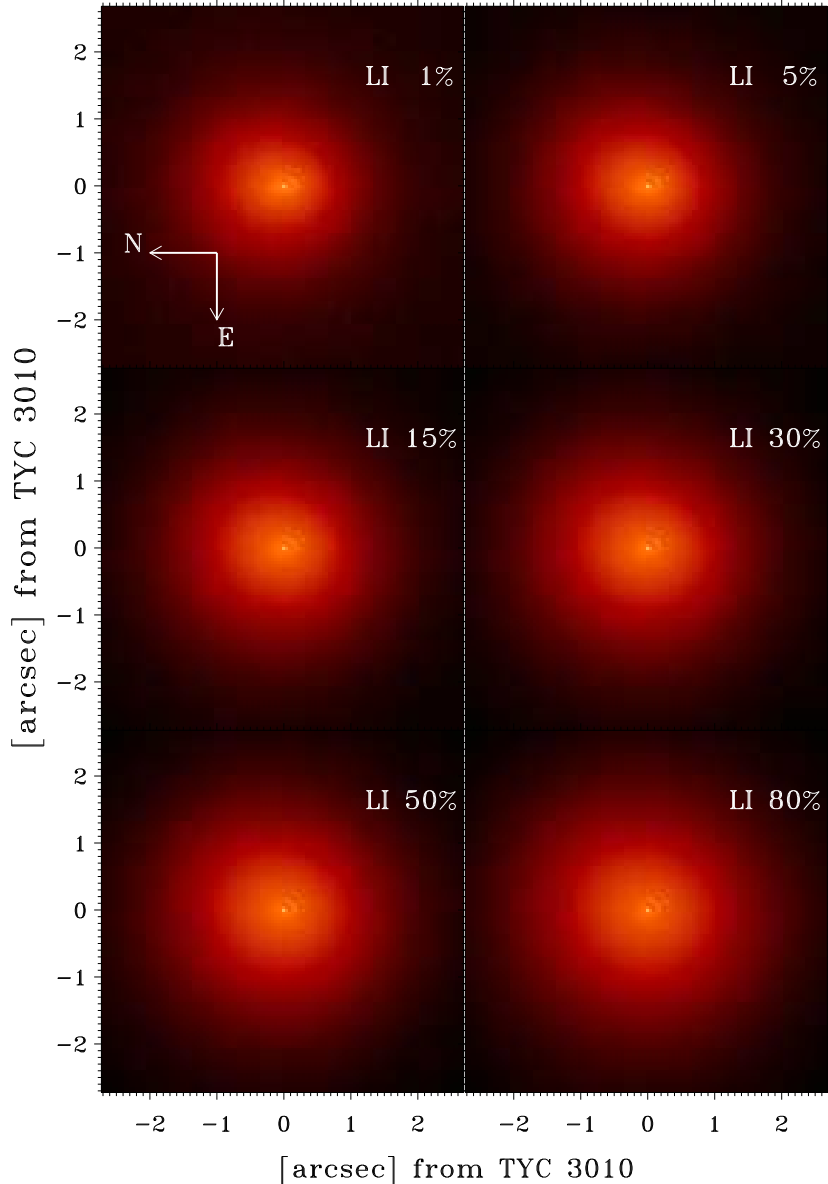


FIG. 4.— The best lucky imaging frames for TYC 3010. The best frames are selected according to the brightest pixel (BP) method as described in Section 2.4.

NextGen models (Hauschildt et al. 1999) are used to generate theoretical SEDs by holding T_{eff} , $\log g$, and $[\text{Fe}/\text{H}]$ at the spectroscopically determined values (see below), and the maximum extinction A_V was limited to 0.05 mag based on the dust maps of Schlegel et al. (1998). The best fit model can be seen in the top panel of Figure 6; it corresponds to an A_V of 0.035 ± 0.015 , and a distance of 162 ± 35 pc. This single-star SED fit to the available photometry spanning $0.2\text{--}12\mu\text{m}$ is quite good, with the only hint of a discrepancy being a mild excess that appears in the *Galaxy Evolution Explore (GALEX)* near-UV (NUV) passband, despite the lack of any strong emission in the observed Ca HK lines. However, this by itself was not deemed to be a compelling reason to suspect the high quality orbit solution.

Thus, at this point in our analysis, fully 38 RV measurements from two separate instruments were well fit by the same orbit solution of a single, solar-type star with a $\sim 50 M_{\text{Jup}}$ companion on a modestly eccentric

orbit. The SED of TYC 3010 was furthermore consistent with being a single solar-type star, and the lack of any companions in the high-resolution imaging ruled out a blend scenario in which the RV variations might be caused by a binary beyond $0.5''$ of the line of sight. Only four of the discovery RV measurements appeared to be discrepant, and these were rejected for what appeared to be good reasons, behaving not unlike fiber mis-pluggings that the MARVELS team had observed in other stars before. However, the last two RV measurements from the first set of ARCES observations appeared as strong outliers (see Figure 1, blue points near HJD 2455730). As they were observed with a standard echelle spectrograph, these could not be attributed to fiber mis-pluggings, and inspection of the CCFs revealed double lines (see bottom panel of Figure 3), immediately nullifying the BD companion hypothesis.

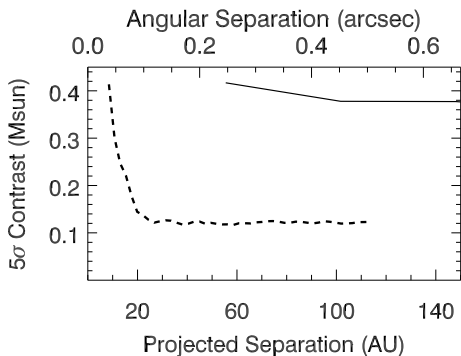


FIG. 5.— Detectability (contrast curve) for the lucky imaging (solid) and Keck AO (dashed) images obtained for TYC 3010. Given the lucky imaging and AO detection limits, we can derive an upper limit (5σ) on the mass of companions as a function of angular separation. With this upper limit, we can rule out the presence of companions above a mass of $\sim 0.35 M_{\odot}$ outside of ~ 50 AU, and above a mass of $\sim 0.13 M_{\odot}$ outside of ~ 100 AU.

3.2. Final solution: A highly eccentric, double-lined spectroscopic binary

To further confirm that TYC 3010 was indeed a stellar binary, we closely observed the next peripassage with the HRS spectrograph on HET. With HET, we obtained complete coverage of periastron, permitting a complete double-lined orbit solution. In this section we present the correct orbit solution for TYC 3010, including all the points from the discovery and subsequent data, which shows that TYC 3010 is an SB2 with a period of $P \sim 238$ days, an eccentricity of $e \sim 0.79$, and a mass ratio of $q \sim 0.88$. With this eccentricity and orbital period, TYC 3010 lies near the upper bound of (but within) the distribution of orbital eccentricities of solar-type binaries with orbital periods of 100–300 days (see, e.g., Duquennoy & Mayor 1991; Raghavan et al. 2010). The orbital parameters for the binary are summarized in Table 4, the RV solution is shown in Figure 7, and a schematic of the orbit is shown in Figure 8. In this section we also describe our determination of the stellar parameters for the primary in TYC 3010, and we estimate its mass and radius using the relations described in Torres et al. (2010). Since the secondary is comparable in mass to the primary, we had to take special care in accounting for the flux contamination from the secondary, both in our determination of the stellar parameters and with the RV values that we measured for the system outside of periastron.

3.2.1. RV fitting

For the orbital solution of the binary, we used the RV fitting software described in Gudehus (2001). Since we do not resolve two sets of spectral lines for the phases outside of periastron, most of the RV points correspond to a flux-weighted average of the primary and secondary RVs. In order to de-blend the flux-weighted RVs that we measured, and derive the corresponding primary RVs, we used the following prescription.

We treat the blended velocities as a flux-weighted average of the primary and secondary velocities:

$$v_{\text{blend}} = \frac{v_A F_A + v_B F_B}{F_A + F_B}, \quad (1)$$

where v_A and v_B are the primary and secondary veloc-

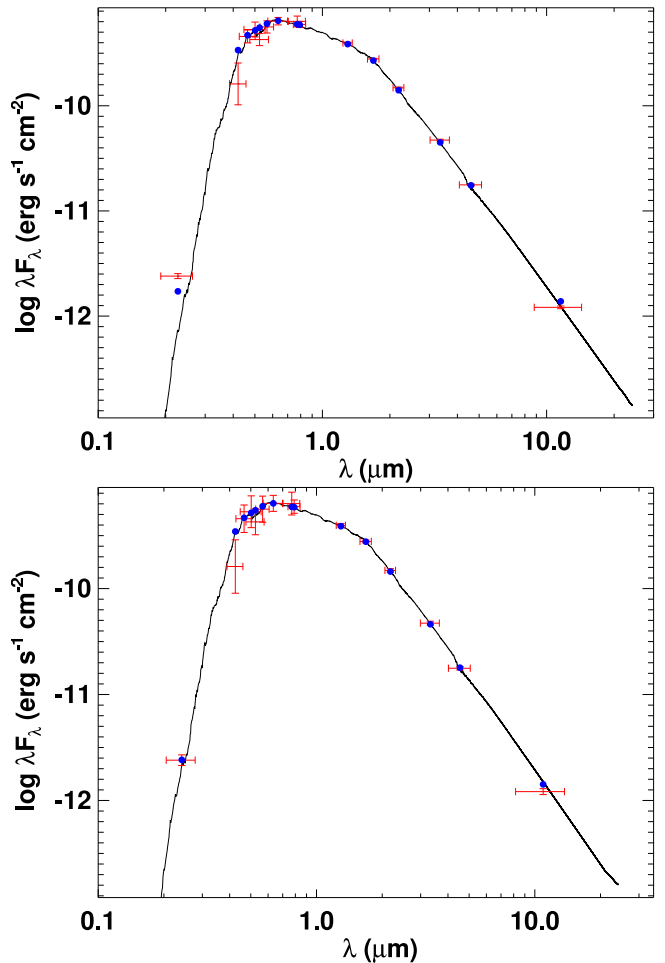


FIG. 6.— *Top*: A NextGen model atmosphere (solid line) fit to the observed broadband fluxes for TYC 3010 (assuming a single stellar component). The blue points are the flux values predicted by the model for the different bandpasses. The vertical red bars correspond to the uncertainties in the measured fluxes, while the horizontal red bars are the approximate widths of the bandpasses. This fit assumed that TYC 3010 was a single star, and found that $T_{\text{eff}} = 5400 \pm 100$ K, $\log g = 4.5 \pm 0.5$, $[\text{Fe}/\text{H}] = 0.0 \pm 0.1$, and $A_V = 0.035 \pm 0.015$, yielding a distance of 162 ± 35 pc. *Bottom*: A second NextGen fit that uses two stellar components (corresponding to the primary and secondary stars of TYC 3010) with one of the components constrained to the spectroscopically determined stellar parameters for the primary ($T_{\text{eff}} = 5589 \pm 148$ K, $\log g = 4.68 \pm 0.44$, $[\text{Fe}/\text{H}] = 0.09 \pm 0.20$). This fit estimates the secondary stellar parameters to be $T_{\text{eff}} = 4600 \pm 850$ K, $R = 0.75 \pm 0.4 R_{\odot}$, $\log g = 4.6 \pm 0.2$, and the distance to TYC 3010 to be 225 ± 40 pc, with an $A_V = 0.03 \pm 0.02$ ($\chi^2/\text{dof} = 0.75$).

ities respectively, and F_A and F_B are the primary and secondary fluxes. We normalize the flux weights by setting the sum of the fluxes, $F_A + F_B$, to unity. Using the flux ratio, $\alpha = F_B/F_A$, from the TODCOR analysis (which was only performed for the HET/HRS epochs where it was possible to resolve two sets of spectral lines), we can solve for F_A and F_B in terms of α :

$$F_A = \frac{1}{1 + \alpha}; \quad F_B = \alpha F_A. \quad (2)$$

In addition, we can use the mass ratio, $q = M_B/M_A$, from the RV solution to write v_B in terms of v_A , since

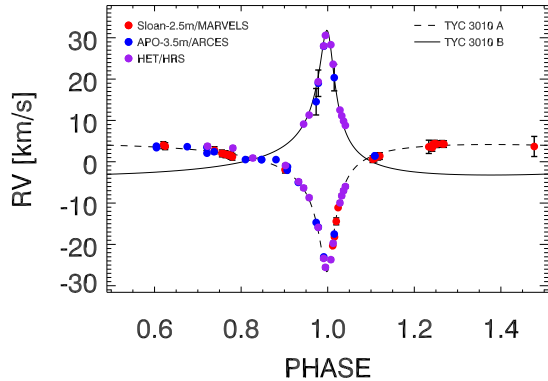


FIG. 7.— The correct phase-folded radial velocity curve for TYC 3010. The best-fit BINARY (Gudehus 2001) orbital solution for the primary (dashed line) and secondary (solid line) are shown with the RVs obtained from the MARVELS (red), ARCES (blue), and HRS (purple) spectrographs. This solution corresponds to a period of ~ 238 days, an eccentricity of ~ 0.79 , with $K_1 \sim 15.38 \text{ km s}^{-1}$ and $K_2 \sim 17.50 \text{ km s}^{-1}$. Finally, for the RV points outside of periastron, it was necessary to de-blend the observed RVs with the method described in Section 3.2.1.

$$M_B/M_A = v_A/v_B.$$

$$v_B = -v_A \left(\frac{M_A}{M_B} \right) = \frac{-v_A}{q} \quad (3)$$

Returning to (1), we can now write

$$v_A = \frac{v_{\text{blend}}}{F_A - F_B/q} = \left(\frac{1 + \alpha}{1 - \alpha/q} \right) v_{\text{blend}} \quad (4)$$

With Equation (4), we can iteratively solve for a final set of de-blended RVs for the primary. For the first iteration, we provide an initial guess for q by performing a joint fit to the primary RVs (blended+unblended) combined with the secondary RVs (unblended; only measured during periastron). Inserting this initial guess for q into Equation (4), we derive an initial set of de-blended primary RVs. Then we perform another joint fit to the primary (de-blended+unblended) and secondary (unblended) RVs to refine our value for q . We repeat the process until q converges. The value we find for q (0.878 ± 0.016) from this de-blending analysis is in excellent agreement with the value for q (~ 0.88) that we found from the ratio of the primary and secondary RVs that were measured for the 11 HET/HRS epochs where two peaks were resolved in the CCFs. Thus, q has been determined very precisely by the orbital solution (better than 3%), and is more precise than the individual quoted errors on the masses.

As a further consistency check on α and q , we also note that according to the relationship between mass and bolometric luminosity from Torres et al. (2010), there should be a relationship between α and q . Since α is derived from a set of finite wavelength bands, it is not bolometric. However, since the stars have temperatures that are not too dissimilar, α is likely to be approximately equal to the ratio of the bolometric luminosities. For stars with $M = 0.6 - 1.2 M_\odot$, a fit to the Torres et al. (2010) data yields $L \propto M^{5.1}$. Thus, $\alpha = q^{5.1}$, so $q \sim (0.335)^{1/5.1} \sim 0.81$, which is within 3σ of the value

TABLE 6
TYC 3010 PROPERTIES DERIVED BY THIS WORK

System Properties		
Parameter	Value	Uncertainty
$\alpha = F_B/F_A$	0.335	0.035
$q = M_B/M_A$	0.878	0.016
A_V	0.03	0.02
d (pc)	225	40
TYC 3010 A		TYC 3010 B
T_{eff} (K)	5589 ± 148	4600 ± 850
$\log g$ (cgs)	4.68 ± 0.44	4.60 ± 0.20
[Fe/H]	0.09 ± 0.20	...
M (M_\odot)	$1.04^{+0.15}_{-0.12}$	$0.73^{+0.24}_{-0.23}$
R (R_\odot)	$0.75^{+0.54}_{-0.27}$	$0.68^{+0.23}_{-0.18}$

NOTE. — The properties for the primary were determined by the spectroscopic stellar parameters and the Torres et al. (2010) relations. The properties for the secondary were determined from the stellar parameters found by the two-component fit to the SED and the Torres relations.

obtained from the RV analysis.

3.2.2. Determining the stellar parameters for TYC 3010

The stellar parameters for the primary were determined with a double-lined spectrum obtained near periastron (see Section 2.2). The spectroscopic analysis used to determine the atmospheric parameters is similar to the one described in Wisniewski et al. (2012), where we use two independent methods that require the conditions of excitation and ionization equilibria for Fe I and Fe II lines. These methods are referred to as the “BPG” (Brazilian Participation Group) method and the “IAC” (Instituto de Astrofísica de Canarias) method.

The “BPG” analysis was done in local thermodynamic equilibrium (LTE) using the 2002 version of MOOG¹ (Sneden 1973) and one-dimensional plane-parallel model atmospheres interpolated from the ODFNEW grid of ATLAS9 models (Kurucz 1993; Castelli & Kurucz 2004). In previous MARVELS papers (e.g., Wisniewski et al. 2012, and references therein), the equivalent widths (EWs) of the Fe lines were determined in an automated fashion. However, in this case, the EWs were manually measured to carefully account for visible blends on the Fe lines from the secondary’s spectrum. We note that contaminations from very weak lines could have affected the EW measurements. In order to correct the EWs measured for the primary for the veiling from the continuum flux of the secondary star, we followed a procedure similar to the one described in Section 5.2.1 of González Hernández et al. (2008). According to their prescription, we can relate the value of the true equivalent width (EW_{true}) of a given line to the observed equivalent width (EW_{obs}) through the following relationship,

$$EW_{\text{true,A}} = f_A (EW_{\text{obs,A}}) \quad (5)$$

where f_A is the so-called veiling factor for the primary. The veiling factors for the two components are related by

$$\frac{f_B(\lambda)}{f_A(\lambda)} = \frac{F_A(\lambda)}{F_B(\lambda)} = \frac{1}{\alpha}, \quad (6)$$

¹ <http://www.as.utexas.edu/~chris/moog.html>

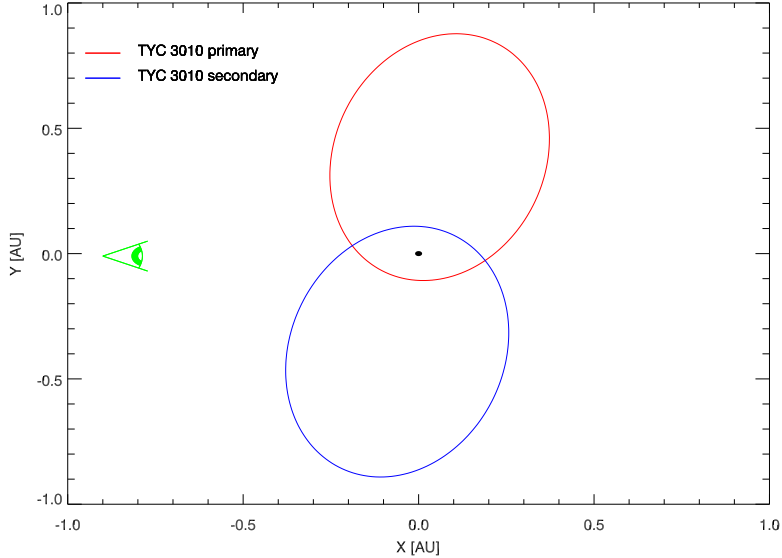


FIG. 8.— A schematic of the TYC 3010 system drawn to scale, showing the primary (red) and secondary (blue) orbits in the orbital plane. The position of the center of mass of the system is marked by the black point. Given the eccentricity ($e \sim 0.79$) and the fact that the semi-major axis is aligned nearly perpendicular to the line of sight ($\omega \sim 189^\circ$), for a substantial fraction of the orbit the system can mimic the RV signal that would normally be induced by a secondary object with a minimum mass in the brown dwarf regime. Coupled with the relatively long period (~ 238 days), depending on the frequency of the observations, it can be fairly easy to miss peripassage during a given orbit.

where F_A and F_B are the fluxes for the primary and secondary. Furthermore, the veiling factors satisfy the equation

$$\frac{1}{f_A(\lambda)} + \frac{1}{f_B(\lambda)} = 1 \quad (7)$$

To simplify our analysis, we treated the veiling factors and flux ratio as if they were wavelength independent. Using the average flux ratio derived by TODCOR ($\alpha = F_B/F_A = 0.335 \pm 0.035$; see Section 2.3.2), and the added constraint from Equation 7, we find the veiling factor for the primary to be $f_A \sim 1.34$. Thus, after correcting the EWs, we find the stellar parameters to be $T_{\text{eff}} = 5589 \pm 148$ K, $\log g = 4.68 \pm 0.44$, and $[\text{Fe}/\text{H}] = 0.09 \pm 0.20$ (see Table 6). The uncertainties for these parameters are larger than the typical errors that we achieve with our spectroscopic analysis because of the flux contamination from the secondary star.

The ‘‘IAC’’ analysis extracted the stellar parameters of the primary and secondary stars by considering veiling factors that were wavelength-dependent. These veiling factors are estimated using low-resolution Kurucz fluxes (Allende Prieto & Lambert 2000, and references therein) and the following equation:

$$\frac{f_B(\lambda)}{f_A(\lambda)} = \frac{\Gamma_A(\lambda)}{\Gamma_B(\lambda)} \left(\frac{R_A}{R_B} \right)^2, \quad (8)$$

where Γ_A and Γ_B correspond to the surface brightness of the primary and the secondary respectively. To determine the ratio of the radii, we derived an empirical mass–radius relationship from a sample of 55 stars from Torres et al. (2010), with the masses restricted to $0.7 M_\odot < M < 1.4 M_\odot$. We fit a function to the data of the form

$$\log R/R_\odot = a \log(M/M_\odot) + b, \quad (9)$$

where $a = 1.052 \pm 0.097$ and $b = 0.036 \pm 0.008$. Thus, the ratio of the radii for the components of TYC 3010 can be written as

$$R_A/R_B = \left(M_A/M_B \right)^{1.052} \quad (10)$$

The mass ratio was determined from the TODCOR analysis to be $q = M_B/M_A \sim 0.88$, so we find that $R_A/R_B = 1.142$.

As a first guess, we adopt the above values to estimate the stellar mass and radius of the primary (Allende Prieto et al. 2004; Reddy et al. 2006; Ramírez et al. 2007), from solar-scaled theoretical isochrones (Bertelli et al. 1994). The mass ratio allows us to derive a first guess of the $T_{\text{eff},B}$ value for the secondary to be roughly 5100 K, assuming $\log g \sim 4.70$ and the same metallicity as the primary. The stellar radii we get from the comparison with isochrones are $0.89 R_\odot$ and $0.77 R_\odot$, and thus the ratio is $R_A/R_B = 1.145$, which is very similar to the value previously estimated ($R_A/R_B = 1.142$). Thus, the derived veiling factors lie in the range $f_{\lambda,A} \sim 1.45 - 1.55$ and $f_{\lambda,B} \sim 3.20 - 2.85$ in the spectral region 4500–7000 Å.

We then measure automatically, using the code ARES (Sousa et al. 2007), the EWs of the Fe I and Fe II lines (Sousa et al. 2008) for both stellar components and correct them using the wavelength-dependent veiling factors. We then use the code STEPAR (Tabernero et al. 2012) to automatically derive the stellar parameters of each component and we get $T_{\text{eff},A} = 5410 \pm 124$ K, $\log g_A = 4.57 \pm 0.56$, $[\text{Fe}/\text{H}]_A = 0.02 \pm 0.20$ and $\xi_A = 0.90 \pm 0.22$ from 162 Fe I and 18 Fe II lines. The uncertainties are unexpectedly large and may be due to the contamination of neighboring lines of other elements of the companion star. Thus the results for the secondary are fairly tentative and the errors are even larger. We were only able to measure 64 Fe I and 3 Fe II lines

to get $T_{\text{eff},B} = 5136 \pm 323$ K, $\log g_B = 4.71 \pm 0.88$, $[\text{Fe}/\text{H}]_B = -0.15 \pm 0.26$ and $\xi_B = 0.75 \pm 0.40$. Compared to the ‘‘BPG’’ analysis, the lower $T_{\text{eff},A}$ of the primary may be related to the different methods used to derive the veiling factors. Nevertheless, the ‘‘IAC’’ stellar parameters for the primary star are very similar to those previously derived and are actually consistent within the large uncertainties so we decide to adopt the ‘‘BPG’’ values.

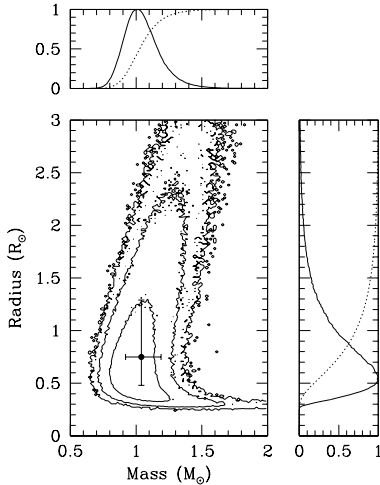


FIG. 9.— Mass and radius distributions for the primary component of TYC 3010. These distributions were determined by a set of MCMC trials with the spectroscopic stellar parameters and the empirical relations from Torres et al. (2010). The black point represents the median ($M_* = 1.04^{+0.15}_{-0.12} M_\odot$, $R_* = 0.75^{+0.54}_{-0.27} R_\odot$), and the error bars correspond to the 68.27% confidence intervals. The contours are lines of equal probability density which enclose 68%, 90%, and 95% of the cumulative probability relative to the maximum of the probability density. In the top and right panels, the probability distribution (solid line) and cumulative probability (dashed line) are shown for the mass and radius respectively.

With the ‘‘BPG’’ stellar parameters for the TYC 3010 primary, we again performed a fit to the observed SED of the system as in Section 3.1, but now also including the contribution of the secondary star. Once again, NextGen models (Hauschildt et al. 1999) are used to generate theoretical SEDs by holding T_{eff} , $\log g$, and $[\text{Fe}/\text{H}]$ at the spectroscopically determined values for the primary, while the T_{eff} for the secondary is found by the value that minimizes χ^2 ($\chi^2/\text{dof} = 0.75$). The best fit model can be seen in the bottom panel of Figure 6; it corresponds to an A_V of 0.03 ± 0.02 , and a distance of 225 ± 40 pc. Compared to the SED fit performed in Section 3.1, which assumed a single stellar contribution, this two-component SED fit no longer exhibits an excess in the *GALEX* NUV passband, and more generally is an excellent fit to all of the available photometry. Finally, from this two-component fit to the SED, we also obtain a set of values for the stellar parameters of the secondary of TYC 3010. We find that $T_{\text{eff}} = 4600 \pm 850$ K, $\log g = 4.6 \pm 0.2$, and $[\text{Fe}/\text{H}] = 0.05 \pm 0.19$.

3.3. Inferred evolutionary status of TYC 3010

Given the spectroscopic stellar parameters, we can derive the mass and radius of the TYC 3010 primary star using the empirical relationships described

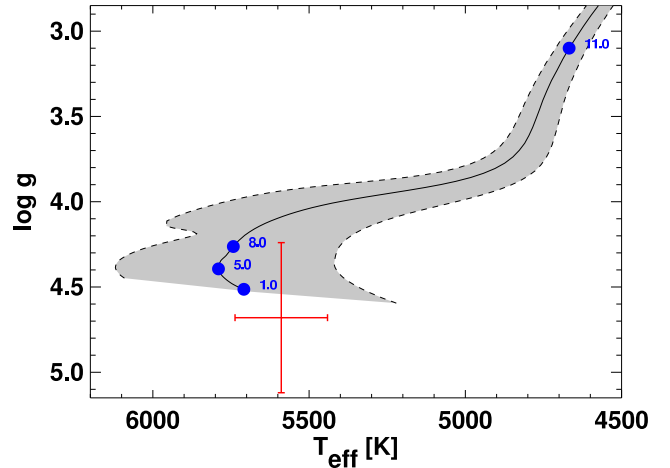


FIG. 10.— H-R diagram that compares the derived stellar parameters for the primary of TYC 3010 (red error bars) to a Yonsei-Yale stellar evolutionary track (solid curve; Demarque et al. 2004) for a star with a mass of $1.04 M_\odot$ and $[\text{Fe}/\text{H}] = 0.09$. Ages (in Gyr) of 1.0, 5.0, 8.0, and 11.0 are represented by blue dots, and the 1σ deviations from the evolutionary track are shown in the shaded region.

in Torres et al. (2010). Figure 9 shows the result of a set of MCMC trials for the best estimate of the mass and radius. For the precise parameters of the primary ($T_{\text{eff}} = 5589$ K, $\log g = 4.68$, $[\text{Fe}/\text{H}] = 0.09$), the Torres relations give $0.98 M_\odot$ and $0.75 R_\odot$. Once one includes the fairly large uncertainties in the stellar parameters, the median values for the mass and radius become $1.04^{+0.15}_{-0.12} M_\odot$ and $0.75^{+0.54}_{-0.27} R_\odot$, respectively. The means are $1.05 \pm 0.15 M_\odot$ and $0.90 \pm 0.54 R_\odot$, so the distributions are quite skewed as shown in Figure 9. Compared to a Yonsei-Yale evolutionary track (see Figure 10), we do not have a strong constraint on the age, but TYC 3010 is unlikely to have evolved off the main sequence.

We can also derive the mass and radius for the secondary given the stellar parameters determined from the two-component SED fit and the Torres et al. (2010) relations. We find that $M_B = 0.74^{+0.26}_{-0.23} M_\odot$ and $R_B = 0.76^{+0.27}_{-0.19} R_\odot$. This value for the mass of the secondary agrees within 1σ of the value that can be derived using the primary mass we determined above and the mass ratio from the RV solution, i.e., $M_B \sim 0.89 M_\odot$.

4. DISCUSSION

4.1. Why we initially derived a spurious solution

The RV signal from TYC 3010 initially seemed to indicate that it was a BD orbiting a solar-type star in the BD desert. Over 80% of the MARVELS discovery data agreed with this interpretation, and there seemed to be plausible reasons for excluding the outliers. However, once similar outliers were found in the subsequent observations, we began to suspect the validity of the BD interpretation. In this section, we discuss in detail why we initially favored the BD interpretation, as well as how this conclusion was abruptly overturned by a few surprising data points.

In the discovery data, there were four outliers in total, each offset by ~ 20 km s $^{-1}$ from the rest of the data. The most anomalous of the outliers was extracted from a spectrum with a low S/N, so its RV value did not seem trustworthy. The remaining outliers (considering that

they corresponded to a $\sim 20 \text{ km s}^{-1}$ offset in RV that was only captured once during the three orbits contained in the discovery data), also seemed likely to be spurious. The MARVELS spectrograph is a fiber-fed spectrograph that can observe 60 objects simultaneously. Each fiber is plugged by hand to observe the correct target, and occasionally a mistake may occur. Indeed, the MARVELS data vetting procedures were evolved to specifically include an outlier rejection step that sought to mitigate such errors, by searching for consecutive strings of measurements that were offset from the bulk of the data in a similar fashion to how these four measurements behave.

Remarkably, excluding these few apparent “outliers”—and in fact *only* by excluding them—permits a convincing orbit solution. It is not intuitive that this should be the case, in particular because only $\sim 15\%$ of the measurements are excluded (including both the discovery data and the initial follow-up data which appeared to corroborate the spurious solution) and because the resulting solution is so dramatically different from the true solution. Evidently, a system such as TYC 3010 (with its extreme eccentricity, leading to punctuated large RV excursions, and its orbital orientation being nearly perpendicular to the line of sight, leading to very small RV variations for $\sim 95\%$ of the orbit) is able to mimic a more circular orbit of a low-mass companion about a single star. Moreover, the similarity of the two stars in TYC 3010 leads to a combined light SED that is only slightly different from that of a single star at a nearer distance.

Thus many lines of evidence supported the initial solution, considering that the BD interpretation appeared to be supported by two years of discovery RV data, six months of additional RV observations, lucky imaging, and a well-constrained SED. Indeed, when the two follow-up RV measurements observed near periastron appeared, indicating a possible problem with the original orbit solution, we began to search for reasons to suspect the validity of these two anomalous points. At first, we thought the situation might be similar to the fiber mispluggings believed to have occurred with the discovery data, and we considered that the ARCES outliers were the result of pointing at the wrong star. But after investigating the data from those two nights, we confirmed that we had observed the correct target. Next we learned of a recent change that had been made to the ARCES instrument: the ThAr lamp had recently been replaced. The ThAr lamp is used to perform the wavelength calibration, and it was plausible that the new lamp might have caused problems with the wavelength solution. Therefore, the ARCES outliers may have merely been the result of an artificial Doppler shift generated by an incorrect wavelength solution. In the end, we were only able to accept that the BD interpretation was incorrect after we inspected the CCF for each of the outliers. The CCFs for the outliers both showed two peaks instead of one, indicating the presence of a second stellar component. Furthermore, the secondary peak was comparable in height to the primary peak (see bottom panel of Figure 3), which led us to suspect that TYC 3010 was in fact a spectroscopic stellar binary.

But how did most of the data that we had for TYC 3010 conspire to imply that it was a much less massive system? The period, shape, and orientation of the orbit with respect to the line of sight (see Figure 8) made

it such that for most of the orbit the two stars possess relatively low RVs with respect to each other. In particular, the difference between the magnitude of their RVs is smaller than the typical CCF width for our instruments, resulting in their CCF peaks being blended into one. Since the flux ratio is not too different from unity, and the mass ratio is also close to unity, for epochs where the spectral lines are blended, there is a near-cancellation (or strong suppression) of the true orbital velocities for the primary and secondary, which are nearly equal in magnitude but oppositely signed (see Equation 4, and recall that v_{blend} is what we actually measure). Thus, for $\sim 95\%$ of the orbit, the amplitude of the variations ($\sim 1\text{--}2 \text{ km s}^{-1}$) suggest a BD companion to a solar-type star; furthermore, the eccentricity and the orbital period ensure that the stars spend a long time (~ 7 months) away from periastron, which is precisely the moment when the RVs of the components are disparate enough for it to be fairly easy to resolve the two sets of spectral lines, and the large RV amplitude ($\sim 15\text{--}20 \text{ km s}^{-1}$) is indicative of a stellar binary with two solar-type stars. Moreover, the orientation makes it so that only a relatively small component of the orbital velocities is directed along our line of sight. Finally, the cadence of the MARVELS survey made it unlikely to observe multiple epochs of periastron.

4.2. How RV surveys can identify astrophysical false positives like TYC 3010

For any given RV survey, the lower the resolution of the spectrograph, the more vigilant one must be for these kinds of false positives. For TYC 3010 in particular, a spectrograph with a resolution of $R \gtrsim 50,000$ is required to resolve the spectral lines throughout most of the orbit. But in general, as the resolution (and cadence of observations) decreases, the wider the range of eccentricities, arguments of periastron, and orbital periods by which stellar binaries could masquerade as substellar companions for significant fractions of their orbits.

Furthermore, longer period orbits ($P \gtrsim 1 \text{ yr}$) should be handled with special care, for in these cases the phase coverage is more likely to be incomplete. In order to survey $\sim 3,000$ stars over four years, MARVELS required a cadence that made it less likely to observe multiple epochs of periastron for a binary with the period of TYC 3010. For MARVELS and similar RV surveys for substellar companions, it can be costly to use precious resources to examine false positives. Therefore, in this section, we describe a method that the MARVELS team currently employs to identify binaries like TYC 3010 during the candidate-vetting process.

For typical RV surveys today, a standard line bisector analysis can usually be performed to assess the presence of blended double-lined binaries. However, this was not possible for the MARVELS discovery data due to its limited spectral resolution. Thus, following our experience with TYC 3010, MARVELS has developed an internal pipeline for inspecting the widths of the CCF peaks for all of our candidates. This way, we can readily monitor the CCFs for signs that indicate that there may be more than one stellar component present (e.g., the large excursions in the width of the CCF peak that occur near periastron for TYC 3010; see Figure 11). There are two properties of the CCFs that we now monitor: (1) the average width of the CCF peak compared to other stars in

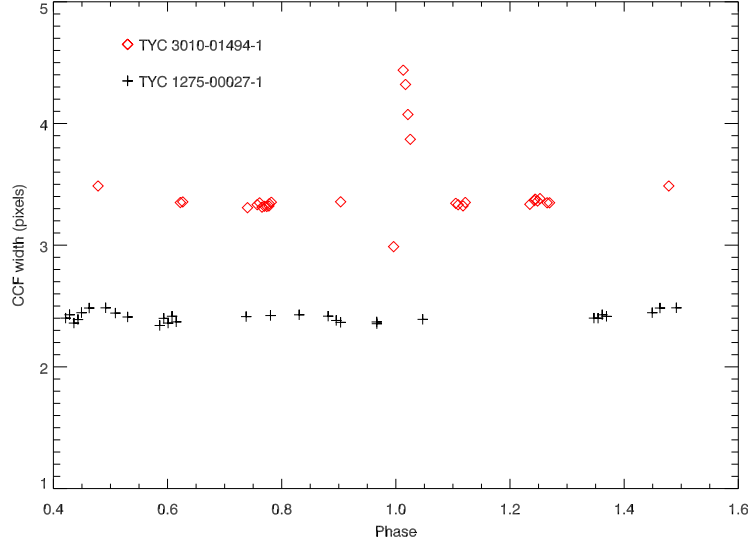


FIG. 11.— A comparison of how the width of the MARVELS CCF peak varies with phase for TYC 3010 (red) and another MARVELS candidate, TYC 1275-00027-1 (black). The MARVELS spectrograph does not possess the resolution to resolve two separate peaks in the CCF for TYC 3010, even at periastron. Instead the width of the CCF broadens dramatically, and upon inspection the peak appears asymmetric with a slight “shoulder” that suggests the presence of an unresolved secondary peak. This large variation in the peak width is not observed in TYC 1275-00027-1, which is known to be a single star. Therefore, by monitoring how the CCF peak changes with phase, and through visual inspection of the peaks, surveys can identify systems that are likely to be false positives like TYC 3010 during the candidate-vetting process. Finally, the median value of the CCF peak width is larger for TYC 3010 than the comparison star, but this may be due to either TYC 3010 rotating faster or the presence of the secondary peak. When confronted with a system whose peak is consistently broader than one might expect for a typical solar-type star, further investigation is necessary to determine if it is merely a fast rotator or if it has a stellar companion.

the survey, and (2) any other significant changes in the shape of the CCF over time.

For a typical solar-type star that is not rotating too rapidly (i.e., the kinds of stars that MARVELS targets), one would expect the width of the CCF peak to be ~ 10 km s $^{-1}$, which is largely the result of thermal broadening and micro-turbulence. However, when binary systems like TYC 3010 are unresolved, the widths of the CCF peak are broader (~ 20 km s $^{-1}$), indicating that there may be multiple stellar components contributing to the flux from the system (see Figure 11). In fact, an atypically broad CCF peak could also be the result of a single star rotating atypically fast, so a broad peak is not in itself sufficient to identify the system as a binary. Nevertheless, a broad peak should be taken as a sign to proceed with caution. Furthermore, changes in the skewness of the CCF peak might provide an even more sensitive diagnostic for these kinds of systems. Thus, by monitoring changes in the CCF peak, even if one misses the small fraction of the orbit where, depending on the resolution, the CCF peak either broadens dramatically or separates into distinct peaks (or if one is suspicious of the relatively few epochs where the system happened to be caught near periastron), it is possible to flag systems like TYC 3010, which may contain much more mass than most of the RV data suggests.

The case of TYC 3010 is also a pertinent lesson on how important it is to handle outliers carefully, especially in this era of large surveys where thousands of objects must be screened for the most favorable candidates. We possessed plausible reasons for suspecting that the outliers in the discovery data might be spurious (known issues with fiber mis-pluggings; low S/N; and the outliers were only

detected during one of the three orbits observed). Moreover, and perhaps ironically, the spurious orbit solution is actually a better fit to the discovery data (excluding the outliers) than the true orbit solution, because of the need to disentangle the primary and secondary RV components from the (apparently) single-lined RV measurements. However, even when faced with such a compelling initial solution and sensible reasons for considering the outliers to be invalid, it is imperative to investigate further and provide evidence that the reasons for rejecting the outliers are not only plausible but justified.

Furthermore, when the analysis is distributed among multiple team members like it is within MARVELS, it is necessary to make sure each step of the analysis is documented as clearly as possible. For MARVELS, the members who perform the candidate-vetting are usually different from those who perform the subsequent analysis for each candidate, so it is important for each team member to be able to readily discover if any outliers were rejected and why. MARVELS has now modified its internal analysis tracking system in order to make the entire analysis process more transparent.

Finally, if we had been monitoring the widths of the CCF peaks, we could have considered the evidence of the broad peak, as well as the changing peak width around periastron, though in truth neither the changing width nor the broad peak by themselves would have likely been sufficiently compelling to reject the initial orbit solution. In the end, the most important part of our analysis was to strategically focus our HET/HRS observations on periastron, the phase where the outliers occurred and where it was easiest to resolve the spectral lines. This strategy would have been more difficult with a conventionally

scheduled telescope, but was readily achieved with the queue-scheduled nature of the HET.

5. SUMMARY

We have demonstrated, using high resolution spectroscopy, that TYC 3010 is an SB2. We have shown how, with a spectrograph below a given resolution ($R \lesssim 50,000$), the eccentricity and the orientation of the system with respect to our line-of-sight allowed a large fraction of the RV curve to appear remarkably similar to the kind of signal one would expect from a BD secondary as opposed to a stellar-mass secondary. Furthermore, as a result of the cadence of the MARVELS survey and the orbital period of the system, we were more likely to miss periastron during a given orbit. Thus, we were more susceptible to rejecting the periastron points we did obtain as outliers, even though these points are where the spectral lines are most widely separated, and thereby where it is easiest to determine that the system is an SB2.

Finally, we concluded with a word of warning to RV surveys, since for a given resolution and cadence, there are a range of orbital parameters that can make a stellar-mass binary companion appear to be substellar. The lower the resolution or cadence, the greater the number of stellar binaries that can masquerade in a fashion similar to TYC 3010. Therefore, if other surveys can carefully monitor the widths of the CCF peaks for their targets (or monitor their line bisectors if they have high enough resolution), and when possible, focus their resources on observations of peripassage, then we hope that they will be able to avoid similar astrophysical false positives.

This research was partially supported by the Vanderbilt Initiative in Data-Intensive Astrophysics (VIDA) and NSF CAREER Grant AST 0349075 (CEM,KGS,LH,JP), NSF AAFP AST 08-02230 (JPW), NSF CAREER Grant AST 0645416 (EA), CNPq grant 476909/2006-6 (GFPM), FAPERJ grant APQ1/26/170.687/2004 (GFPM), NSF CAREER Grant AST-1056524 (BSG,JDE), and a PAPDRJ CAPES/FAPERJ Fellowship (LG).

Based on observations with the SDSS 2.5-meter telescope. Funding for the MARVELS multi-object Doppler instrument was provided by the W.M. Keck Foundation and NSF grant AST-0705139. The MARVELS survey was partially funded by the SDSS-III consortium, NSF Grant AST-0705139, NASA with grant NNX07AP14G and the University of Florida. The Center for Exoplanets and Habitable Worlds is supported by the Pennsylvania

State University, the Eberly College of Science, and the Pennsylvania Space Grant Consortium.

Data presented herein were obtained at the Hobby-Eberly Telescope (HET), a joint project of the University of Texas at Austin, the Pennsylvania State University, Stanford University, Ludwig-Maximilians-Universität München, and Georg-August-Universität Göttingen. The HET is named in honor of its principal benefactors, William P. Hobby and Robert E. Eberly.

This research has made use of the SIMBAD database, operated at CDS, Strasbourg, France, and the AAVSO Photometric All-Sky Survey (APASS), funded by the Robert Martin Ayers Sciences Fund. It also made use of the IRAF software distributed by the National Optical Astronomy Observatory, which is operated by the Association of Universities for Research in Astronomy (AURA) under cooperative agreement with the National Science Foundation. This publication makes use of data products from the Two Micron All Sky Survey, which is a joint project of the University of Massachusetts and the Infrared Processing and Analysis Center/California Institute of Technology, funded by the National Aeronautics and Space Administration and the National Science Foundation. We also make use of data products from the Wide-field Infrared Survey Explorer, which is a joint project of the University of California, Los Angeles, and the Jet Propulsion Laboratory/California Institute of Technology, funded by the National Aeronautics and Space Administration. Funding for SDSS-III has been provided by the Alfred P. Sloan Foundation, the Participating Institutions, the National Science Foundation, and the U.S. Department of Energy Office of Science. The SDSS-III web site is <http://www.sdss3.org/>.

SDSS-III is managed by the Astrophysical Research Consortium for the Participating Institutions of the SDSS-III Collaboration including the University of Arizona, the Brazilian Participation Group, Brookhaven National Laboratory, University of Cambridge, University of Florida, the French Participation Group, the German Participation Group, the Instituto de Astrofísica de Canarias, the Michigan State/Notre Dame/JINA Participation Group, Johns Hopkins University, Lawrence Berkeley National Laboratory, Max Planck Institute for Astrophysics, New Mexico State University, New York University, Ohio State University, Pennsylvania State University, University of Portsmouth, Princeton University, the Spanish Participation Group, University of Tokyo, University of Utah, Vanderbilt University, University of Virginia, University of Washington, and Yale University.

Facilities: Sloan (MARVELS), ARC (ARCES), HET (HRS), Keck:I (NIRC2), Sanchez (FastCam)

REFERENCES

- Allende Prieto, C., Barklem, P. S., Lambert, D. L., & Cunha, K. 2004, *A&A*, 420, 183
 Allende Prieto, C., & Lambert, D. L. 2000, *AJ*, 119, 2445
 Baranne, A., Queloz, D., Mayor, M., et al. 1996, *A&AS*, 119, 373
 Bender, C. F., Mahadevan, S., Deshpande, R., et al. 2012, *ApJ*, 751, L31
 Bertelli, G., Bressan, A., Chiosi, C., Fagotto, F., & Nasi, E. 1994, *A&AS*, 106, 275
 Bouchy, F. e. 2006, in Tenth Anniversary of 51 Peg-b: Status of and prospects for hot Jupiter studies, ed. L. Arnold, F. Bouchy, & C. Moutou, 319–325
 Castelli, F., & Kurucz, R. L. 2004, *ArXiv Astrophysics e-prints*
 Crifo, F., Jasniewicz, G., Soubiran, C., et al. 2010, *A&A*, 524, A10
 Cutri, R. M., Skrutskie, M. F., van Dyk, S., et al. 2003, *VizieR Online Data Catalog*, 2246, 0
 De Lee, N. et al. 2013, submitted
 Delfosse, X., Forveille, T., Ségransan, D., et al. 2000, *A&A*, 364, 217
 Demarque, P., Woo, J.-H., Kim, Y.-C., & Yi, S. K. 2004, *ApJS*, 155, 667
 Duquennoy, A., & Mayor, M. 1991, *A&A*, 248, 485
 Eastman, J., Gaudi, B. S., & Agol, E. 2013, *PASP*, 125, 83
 Eisenstein, D. J., Weinberg, D. H., Agol, E., et al. 2011, *AJ*, 142, 72

- Erskine, D. J. 2003, *PASP*, 115, 255
- Femenía, B., Rebolo, R., Pérez-Prieto, J. A., et al. 2011, *MNRAS*, 413, 1524
- Fleming, S. W., Ge, J., Mahadevan, S., et al. 2010, *ApJ*, 718, 1186
- Fleming, S. W., Ge, J., Barnes, R., et al. 2012, *AJ*, 144, 72
- Ge, J. 2002, *ApJ*, 571, L165
- Ge, J., & Eisenstein, D. 2009, in *ArXiv Astrophysics e-prints*, Vol. 2010, astro2010: The Astronomy and Astrophysics Decadal Survey, 86
- Ge, J., Erskine, D. J., & Rushford, M. 2002, *PASP*, 114, 1016
- Ge, J., van Eyken, J., Mahadevan, S., et al. 2006, *ApJ*, 648, 683
- Ge, J., Mahadevan, S., Lee, B., et al. 2008, in *Astronomical Society of the Pacific Conference Series*, Vol. 398, Extreme Solar Systems, ed. D. Fischer, F. A. Rasio, S. E. Thorsett, & A. Wolszczan, 449
- Ge, J., Lee, B., de Lee, N., et al. 2009, in *Society of Photo-Optical Instrumentation Engineers (SPIE) Conference Series*, Vol. 7440, Society of Photo-Optical Instrumentation Engineers (SPIE) Conference Series
- Girardi, L., Bertelli, G., Bressan, A., et al. 2002, *A&A*, 391, 195
- González Hernández, J. I., Bonifacio, P., Ludwig, H.-G., et al. 2008, *A&A*, 480, 233
- Gudehus, D. H. 2001, in *Bulletin of the American Astronomical Society*, Vol. 33, American Astronomical Society Meeting Abstracts #198, 850
- Gunn, J. E., Siegmund, W. A., Mannery, E. J., et al. 2006, *AJ*, 131, 2332
- Hauschildt, P. H., Allard, F., & Baron, E. 1999, *ApJ*, 512, 377
- Henden, A. A., Levine, S. E., Terrell, D., Smith, T. C., & Welch, D. 2012, *Journal of the American Association of Variable Star Observers (JAAVSO)*, 40, 430
- Henry, T. J. 2004, in *Astronomical Society of the Pacific Conference Series*, Vol. 318, Spectroscopically and Spatially Resolving the Components of the Close Binary Stars, ed. R. W. Hilditch, H. Hensberge, & K. Pavlovski, 159–165
- Henry, T. J., Franz, O. G., Wasserman, L. H., et al. 1999, *ApJ*, 512, 864
- Høg, E., Fabricius, C., Makarov, V. V., et al. 2000, *A&A*, 355, L27
- Jiang, P. et al. 2013, submitted
- Kurucz, R. 1993, *ATLAS9 Stellar Atmosphere Programs and 2 km/s grid*. Kurucz CD-ROM No. 13. Cambridge, Mass.: Smithsonian Astrophysical Observatory, 1993., 13
- Lee, B. L., Ge, J., Fleming, S. W., et al. 2011, *ApJ*, 728, 32
- Lytle, D. M. 1993, in *Astronomical Society of the Pacific Conference Series*, Vol. 52, Astronomical Data Analysis Software and Systems II, ed. R. J. Hanisch, R. J. V. Brissenden, & J. Barnes, 18
- Ma, B. et al. 2013, submitted
- Mamajek, E. 2011, Univ. Rochester internal memorandum. http://www.pas.rochester.edu/~emamajek/EEM_dwarf_UBVIJHK_color_Teff.dat
- Mandushev, G., Torres, G., Latham, D. W., et al. 2005, *ApJ*, 621, 1061
- Marcy, G. W., & Butler, R. P. 2000, *PASP*, 112, 137
- Nidever, D. L., Marcy, G. W., Butler, R. P., Fischer, D. A., & Vogt, S. S. 2002, *ApJS*, 141, 503
- Osoz, A., Rebolo, R., López, R., et al. 2008, in *Society of Photo-Optical Instrumentation Engineers (SPIE) Conference Series*, Vol. 7014, Society of Photo-Optical Instrumentation Engineers (SPIE) Conference Series
- Pepe, F., Mayor, M., Delabre, B., et al. 2000, in *Society of Photo-Optical Instrumentation Engineers (SPIE) Conference Series*, Vol. 4008, Society of Photo-Optical Instrumentation Engineers (SPIE) Conference Series, ed. M. Iye & A. F. Moorwood, 582–592
- Queloz, D., Mayor, M., Weber, L., et al. 2000, *A&A*, 354, 99
- Raghavan, D., McAlister, H. A., Henry, T. J., et al. 2010, *ApJS*, 190, 1
- Ramírez, I., Allende Prieto, C., & Lambert, D. L. 2007, *A&A*, 465, 271
- Ramsey, L. W., Adams, M. T., Barnes, T. G., et al. 1998, in *Society of Photo-Optical Instrumentation Engineers (SPIE) Conference Series*, Vol. 3352, Society of Photo-Optical Instrumentation Engineers (SPIE) Conference Series, ed. L. M. Stepp, 34–42
- Reddy, B. E., Lambert, D. L., & Allende Prieto, C. 2006, *MNRAS*, 367, 1329
- Schlegel, D. J., Finkbeiner, D. P., & Davis, M. 1998, *ApJ*, 500, 525
- Shetrone, M., Cornell, M. E., Fowler, J. R., et al. 2007, *PASP*, 119, 556
- Snedden, C. A. 1973, PhD thesis, THE UNIVERSITY OF TEXAS AT AUSTIN.
- Sousa, S. G., Santos, N. C., Israelian, G., Mayor, M., & Monteiro, M. J. P. F. G. 2007, *A&A*, 469, 783
- Sousa, S. G., Santos, N. C., Mayor, M., et al. 2008, *A&A*, 487, 373
- Taberner, H. M., Montes, D., & González Hernández, J. I. 2012, *A&A*, 547, A13
- Torres, G., Andersen, J., & Giménez, A. 2010, *A&A Rev.*, 18, 67
- Tull, R. G. 1998, in *Society of Photo-Optical Instrumentation Engineers (SPIE) Conference Series*, Vol. 3355, Society of Photo-Optical Instrumentation Engineers (SPIE) Conference Series, ed. S. D'Odorico, 387–398
- van Eyken, J. C., Ge, J., & Mahadevan, S. 2010, *ApJS*, 189, 156
- Wang, J., Ge, J., Jiang, P., & Zhao, B. 2011, *ApJ*, 738, 132
- Wang, J., Ge, J., Wan, X., De Lee, N., & Lee, B. 2012a, *PASP*, 124, 1159
- Wang, J., Ge, J., Wan, X., Lee, B., & De Lee, N. 2012b, *PASP*, 124, 598
- Wang, S.-i., Hildebrand, R. H., Hobbs, L. M., et al. 2003, in *Society of Photo-Optical Instrumentation Engineers (SPIE) Conference Series*, Vol. 4841, Society of Photo-Optical Instrumentation Engineers (SPIE) Conference Series, ed. M. Iye & A. F. M. Moorwood, 1145–1156
- Matthews, K., & Soifer, B. T. 1994, *Astronomy with Arrays, The Next Generation*, 190, 239
- Wisniewski, J. P., Ge, J., Crepp, J. R., et al. 2012, *AJ*, 143, 107
- Wright, E. L., Eisenhardt, P. R. M., Mainzer, A. K., et al. 2010, *AJ*, 140, 1868
- Wright, J. et al. 2013, submitted
- Xia, F., & Fu, Y.-N. 2010, *Chinese Astron. Astrophys.*, 34, 277
- Xia, F., Ren, S., & Fu, Y. 2008, *Ap&SS*, 314, 51
- Zucker, S. 2003, *MNRAS*, 342, 1291
- Zucker, S., & Mazeh, T. 1994, *ApJ*, 420, 806